Chemical Engineering Journal 207–208 (2012) 450–461

Contents lists available at SciVerse ScienceDirect

Chemical Engineering Journal

journal homepage: www.elsevier.com/locate/cej

Bubble columns dynamics inferred from the motion of a radioactive tracer followed by axially aligned detectors

Gabriel L. Salierno [a], María Sol Fraguío [a], Stella Piovano [a], Miryan Cassanello [a,*], María Angélica Cardona [b,c], Daniel Hojman [b], Héctor Somacal [b,c]

[a] PINMATE, Dept. Industrias, FCEyN, Universidad de Buenos Aires, Intendente Güiraldes 2620, C1428BGA Buenos Aires, Argentina
[b] TANDAR, Comisión Nacional de Energía Atómica (CNEA), Centro Atómico Constituyentes, Buenos Aires, Argentina
[c] ECyT, Universidad Nacional de San Martín, San Martín, Argentina

HIGHLIGHTS

- Axially aligned detectors (AADs) allows characterization of bubble columns' dynamics.
- Approximate tracer axial trajectories can be reconstructed from the AADs response.
- Tracer path is analyzed by data symbolization to diagnose flow regime transitions.
- Residence time of the tracer at different column regions is estimated.
- The influence of liquid viscosity on the tracer trajectories is studied.

ARTICLE INFO

Article history:
Available online 20 July 2012

Keywords:
Axially aligned detectors
Radioactive tracers
Flow regimes
Bubble columns

ABSTRACT

Bubble column dynamics can be properly studied with advanced velocimetry techniques, like radioactive particle tracking (RPT). However, sophisticated methods are scarcely used in the industrial environment; simpler methodologies like nuclear gauge scanning are generally preferred even if they provide more limited information. This work explores the feasibility of inferring information of the underlying dynamics in bubble columns, using a set of axially aligned detectors (AADs). The AADs scan simultaneously different column heights when a unique radioactive tracer is left free within the examined vessel, thus avoiding the cumbersome calibration required for RPT. The combined response of the AADs is analyzed by means of a data mining procedure to determine quantitative indexes related to the underlying flow regime.

1. Introduction

Bubble columns are largely used in several processes within the petrochemical, biochemical, metallurgical and chemical industries. Design, scale up and operation of these contactors highly depend on their complex hydrodynamics and the prevailing flow regime [1]. Advanced techniques employing high energy radioactive sources, such as Radioactive Particle Tracking (RPT) or Positron Emission Particle Tracking (PEPT) and computer tomography have proved to be quite appropriate for capturing the underlying dynamics of these inherently opaque contactors, providing features such as liquid velocities, turbulence parameters and phases holdup profiles, that have been used as the input experimental data required for CFD model verification [2,3]. However, their implementation in actual industrial installations is rather complicated, preventing their massive use despite their accessible cost and controllable safety issues. On the contrary, nuclear gauge scanning is more widely applied for equipment diagnostic in the industrial environment, even if the information extracted is more limited. In this context, the objective of this work is to explore the feasibility of inferring information of the underlying dynamics in bubble columns using a set of axially aligned detectors (AADs) when a unique radioactive tracer is introduced in the "observed" vessel, thus avoiding the demanding procedure required for calibration of an RPT facility, which largely complicates its use in the industrial environment. In addition, in contrast to static external sources used for transmission tomography or classical nuclear scanning, a freely moving tracer can capture the dynamics of the phases moving within the vessel. Considering that understanding of the hydrodynamics of bubble columns operated with non-Newtonian fluids still remains to be thoroughly established [4], model non-Newtonian aqueous solutions of carboxymethyl cellulose (CMC) have been used in addition to water.

* Corresponding author.
E-mail address: miryan@di.fcen.uba.ar (M. Cassanello).

1385-8947/$ - see front matter © 2012 Elsevier B.V. All rights reserved.
http://dx.doi.org/10.1016/j.cej.2012.06.150

Table 1
Rheological characteristics of the model liquids employed.

Liquid	k (mPa s^n)	n
Water	1	1
CMC 0.75%	140	0.883
CMC 1.50%	902	0.735

Parameters k and n correspond to the Ostwald-de Waele relation: $\tau = k \cdot (\dot{\gamma})^n$

2. Experimental

Experiments have been carried out in a 1.2 m high and 0.1 m inner diameter acrylic column. The model liquid used, either water or non-Newtonian CMC aqueous solutions of different viscosities, was in batch mode. Table 1 provides details of the model liquids rheological behavior. Filter air was continuously fed from a compressor to impose flow rates within the range of the homogeneous and the heterogeneous flow regimes. Gas velocities varied from 0.005 to 0.125 m/s. The overall gas holdup was also determined by visual inspection of the disengagement region to get the curve of gas holdup vs gas velocity generally used to identify flow transitions in bubble columns [1,5]. In addition, the chordal gas holdup determined, at mid-height of the column, by a standard scanning method with an external radioactive source [3] is also measured to have a more quantitative objective way of determining the gas holdup for different experimental conditions. Even if the chordal gas holdup is a local measure, it captures the holdup trend with gas velocity.

The tracers used to track the liquid motion were prepared by embedding a tiny piece of gold in polyethylene beads to reach the model liquid density. The embedded gold was then activated by neutron bombardment in the RA1 reactor of CNEA to around 80 μCi previous to each series of experiments. The released tracer motion was continuously followed (every 10 ms for about 2 h) by an array of eight $2 \times 2''$ NaI(Tl) scintillation detectors located axially aligned along the column. Fig. 1 illustrates a schematic of the experimental facility.

The combined response of the AADs is analyzed by means of a data mining procedure to reconstruct the approximate axial motion of the tracer and, by applying symbolic dynamics, to produce quantitative indexes related to the underlying flow regime and tracer residence location [6,7].

3. Results

3.1. Tracer axial trajectory

Typical time series of counts simultaneously registered by each of the eight AADs are shown in Fig. 2, for a representative period of 200 s.

The figure evidences high counting rates in all the detectors, being less frequent in detector 8 (D8) at the top of the column, covering the disengagement region. Therefore, the tracer is continuously moving all over the reactor, visiting only occasionally the region at the top of the gas–liquid emulsion. The number of counts determined by each detector depends on its dead time, the media attenuation and mainly on the distance separating the detector crystal from the tracer.

Due to the detectors arrangement and column geometry, it is expected that the detector closest to the tracer in axial coordinate will measure the maximum number of counts provided the counting period is sufficiently short. This assumption is strictly valid if all the detectors have the same size, efficiency and dead time, and the media attenuation is constant. To verify if this assumption still holds under a normal experimental condition, the model developed by Larachi et al. [8] for reconstructing the tracer paths in radioactive particle tracking (RPT) experiments was used to simulate the intensities that will be measured by each detector when the tracer is located at many positions all over the column. For performing the simulation, a calibration was carried out as per normal procedure used for a RPT experiment to get the fitting parameters (detector efficiency, media attenuation and detector dead time). The calibration was done at a high gas velocity, for which the variations in media attenuation along the column are significant due to variations in gas holdup.

Fig. 3 shows the simulated number of counts that would be measured by each detector as a function of the axial coordinate when the tracer is located at 81,000 positions within the reactor. It can be observed that the intensities recorded by the detector which is the closest in axial position are always largely higher than those measured by the others. This is so except for regions in-between two detectors, where there are two detectors measuring similar number of counts and significantly more than all the others. For these conditions, two detectors may even record exactly the same number of counts. Then, an inter-detector region can also

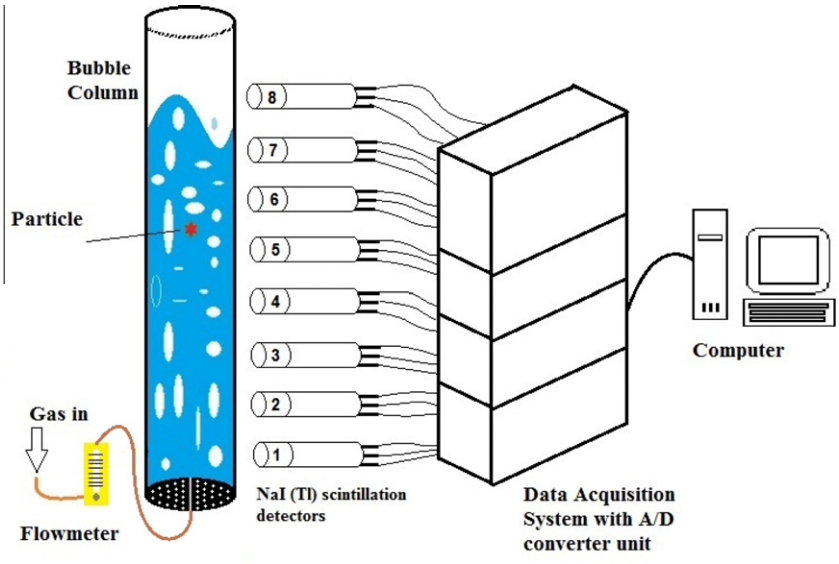

Fig. 1. Schematics of the experimental installation.

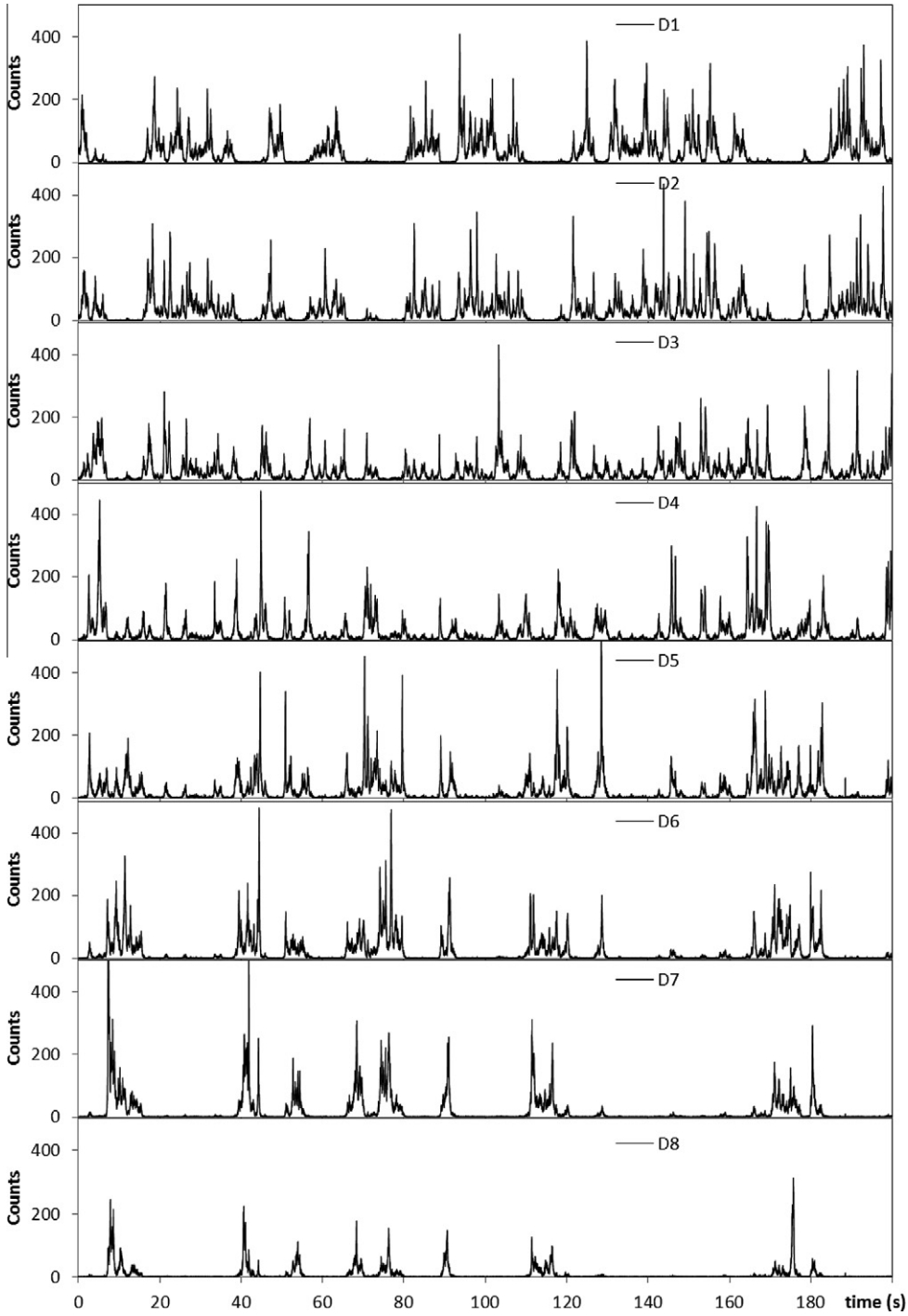

Fig. 2. Typical time series of counts simultaneously registered by each of the 8 AADs. Liquid: water in batch; gas velocity: ug = 0.075 m/s.

be determined from the raw data when intensities of two successive detectors are similar.

Taking into account the results of the simulation that supports the assumptions put forward, the approximate axial location of the tracer (with a maximum resolution of two times the number of detectors minus one) can be directly reconstructed from the raw data by determining the axial location of the two detectors that measure the maximum number of counts. The procedure is to search, at each instant, the detector which measures the maximum number of counts and to normalize all the signals with respect to that value. Then, a threshold is considered to decide if the tracer axial location is assigned to the level of the detector that measures the maximum number of counts or in the middle position between this detector and the second one in the number of counts recorded; from the simulation, the threshold was set in 75% (i.e., if the number of counts measured by the second detector is more than 75% of the maximum the position is assigned to the middle in-between detectors).

The reconstructed discrete axial trajectory of the tracer corresponding to the conditions shown in Fig. 2 is represented in

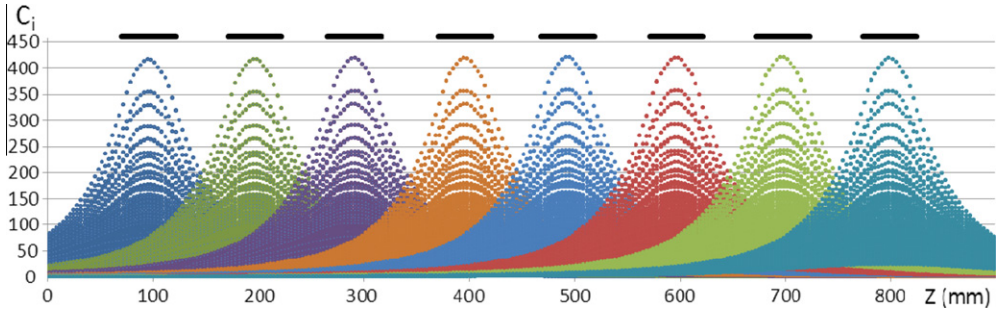

Fig. 3. Simulation of the number of counts registered by each of the 8 AADs when the tracer is located at 81,000 positions within the column. Black line on top indicates axial position spanned by each detector crystal.

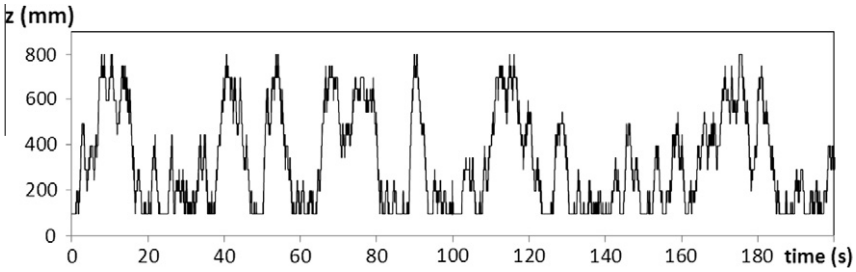

Fig. 4. Typical time series of the tracer approximate axial location determined from the time series of counts shown in Fig. 2. Liquid: water; gas velocity: ug = 0.075 m/s.

Fig. 4, and roughly provides a panorama of the tracer axial motion. This motion represents the liquid axial motion and it is naturally related to the gas velocity and the underlying flow regime.

The frequency of finding the tracer at different axial locations in the column, calculated directly from the frequency of having a maximum for each detector, is illustrated in Fig. 5 for the three model liquids examined and for three gas velocities. Since the tracer is neutrally buoyant, it represents the liquid; hence, Fig. 5 provides an estimation of the liquid axial holdup profile in the column.

For gas velocities below 0.06 m/s, the frequency of finding the tracer close to detector 8 is very low and for the lowest velocities almost nil due to the liquid level. For higher gas velocities, the number of events in the disengagement region increases but it is always less than the number in the rest of the column. The number of events close to the distributor at the column entrance region leads to a frequency of around 20%, higher than the frequency in the rest of the column where it is always between 10% and 15%. It should be noted that the lowest region, covered by detector D1, is larger than the others because there is no detector below; all locations between $z = 0$ and $z = 150$ mm are likely to give a maximum number of counts for detector 1. The regions covered by detectors 2–7 are of 100 mm (e.g., from $z = 150$ mm to $z = 250$ mm for detector 2 and so forth). The profiles show a moderately decreasing trend along the axial coordinate and it is neither strongly dependent on the gas velocity nor on the liquid viscosity.

3.2. Symbolic analysis

The symbolic analysis of experimental time series has been employed in the last decade for classifying dynamic states and for monitoring [6,7,9–12]. Briefly, the experimental time series is converted into a succession of symbols following certain criteria. Afterwards, the symbol sequences are analyzed to search for recurrent patterns and to get fingerprints of the underlying dynamic state. Two approaches are generally followed, either by defining the symbols from a static or a dynamic viewpoint.

3.2.1. Static symbolization

To generate the series of symbol sequences, the time series of tracer axial positions are converted into a series of symbols according to the tracer location in the bed. Taking into account that there are eight detectors inspecting axially the column, eight regions in the bed have been considered. It should be mentioned that the division is arbitrary, the number of regions can be chosen differently; in this case, we decided to select eight regions in order to use directly the raw data. Hence, to get the symbols, the measured intensities are inspected directly to search for the detector that received the maximum number of counts for a given instant. That detector is assigned with a number 1, while the others are assigned with a 0. Groups of eight successive observations are then analyzed to get symbols, which are strongly related to the tracer axial location in the bed. All the regions having a maximum in any of the examined instants are assigned a number 1 and those not explored by the tracer are assigned with a 0. Again, in this case, the group of observations does not need to be eight; the number of observations is related to the window of observation to diagnose a symbol; eight instants imply observing the tracer path for 0.08 s. The observation length is related to the tracer motion time scale. If it is too short, the tracer will rarely move from one region and if it is too long, the tracer may recirculate the column and blurred the analysis.

Having eight regions, 2^8 symbol sequences are defined (binary numbers from 0 to 255). Fig. 6 shows the histograms of symbols occurrences for experiments with water at three gas velocities. The symbol indexes used in the figure are the decimal representation of the binary numbers given by the symbol sequences. Many symbols are forbidden since the particle is always in a certain location in the bed, thus eliminating the zero (00000000), and it is hardly possible to have the tracer in more than 4 regions (symbols with more than 4 ones) if the observation time does not allow the tracer to traverse the whole column. In addition, there are not symbols with zeros between ones because the frequency of observation is high (100 Hz) and the tracer velocity is not high enough to cross entirely a region (around 0.1 m) in 0.01 s.

The relative frequency of the symbols is related to the intensity of the tracer axial motion. Since the velocity of the tracer motion is

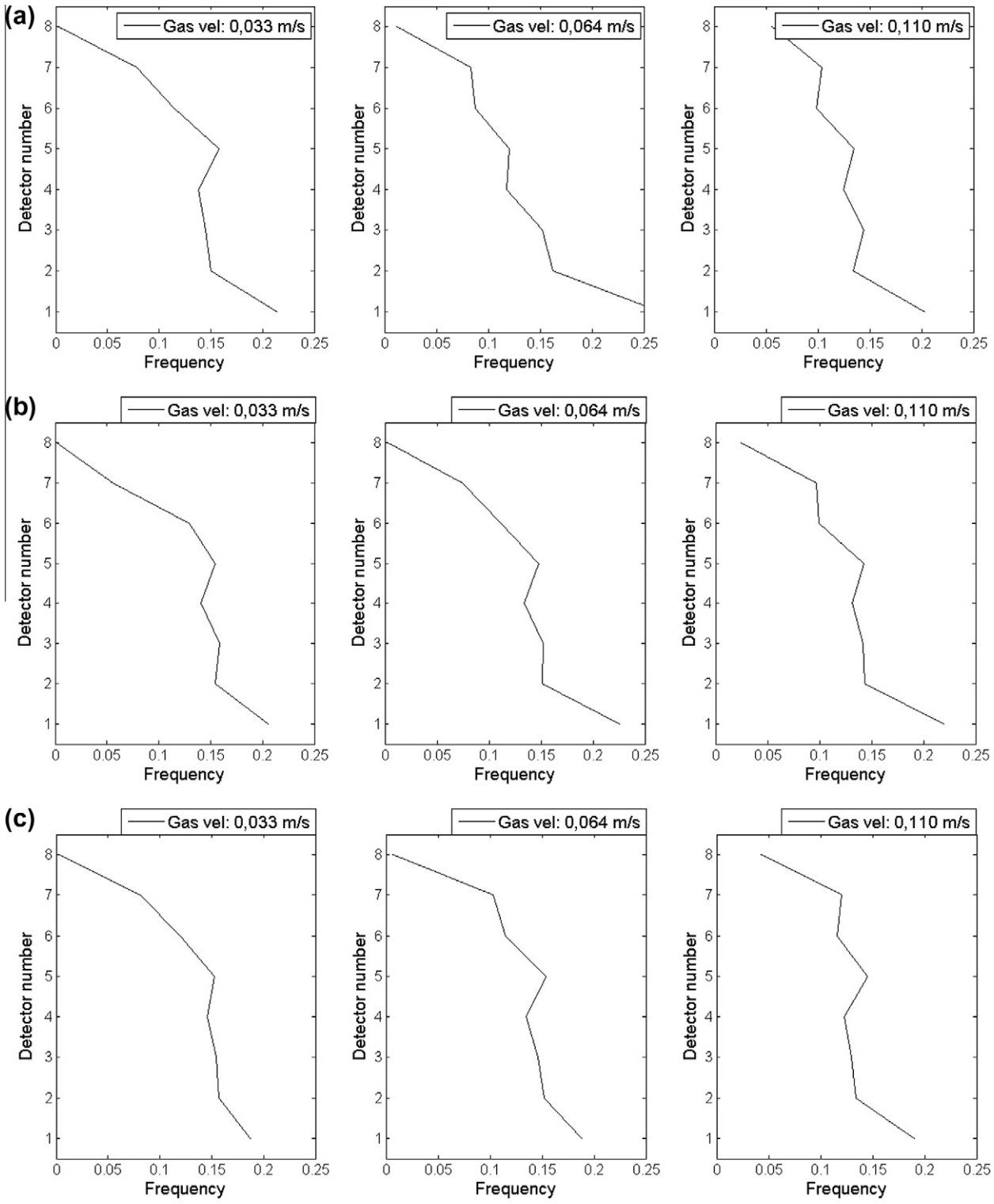

Fig. 5. Frequency of finding the tracer at different axial positions within the column for the model liquids examined and three gas velocities. (a) water, (b) 0.75% w/w CMC, (c) 1.5% w/w CMC.

closely dependent on the gas velocity, two variations are expected as the gas velocity increases: (i) an increase in the frequency of symbols which contain more ones, related to the possibility of finding the tracer within a larger range of axial positions in the column, and (ii) the appearance of symbols with a one associated with the tracer position observed by the detector located in the upmost axial position, related to the liquid level in the column, and therefore to the gas holdup since the liquid volume at rest is kept constant.

To search for a flow transition, it is possible to compare the frequency of a particular symbol and to follow its trend with gas velocity. For instance, Fig. 7 illustrates the frequencies of symbol 192 (11000000), which depend on gas velocity for both reasons (i) and (ii), calculated from experiments with water and the CMC

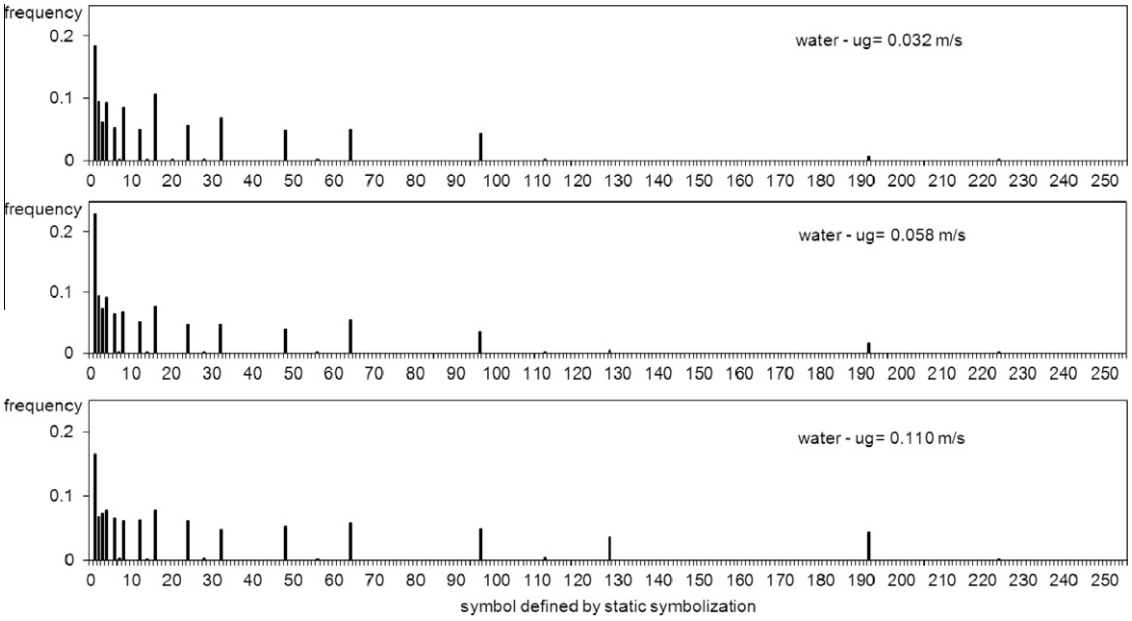

Fig. 6. Histograms of the frequency of appearance of symbols defined according to the static symbolization rule. Liquid: water in batch and three representative gas velocities.

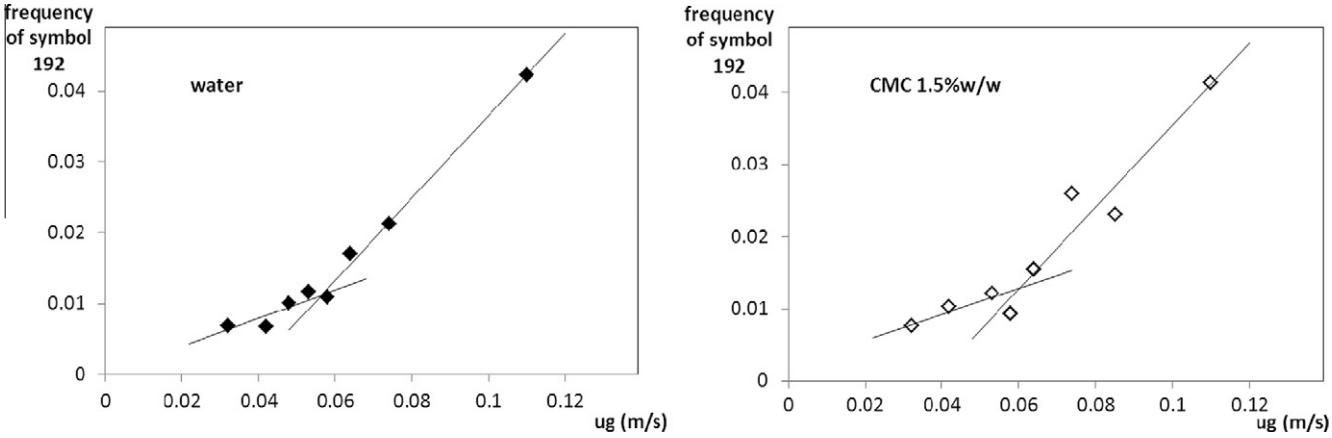

Fig. 7. Trend of the frequency of appearance of symbol 192 (11000000) defined according to the static symbolization rule. Solid lines are only to guide the eyes for remarking the break in the trend.

solution of higher viscosity. This result is an indirect indication of the increase in gas holdup, arising from bed expansion. From the figure, a break in the trend of this symbol with gas velocities seems to appear around 0.06 m/s. For water, the break is observed at a gas velocity slightly below this limit while for the viscous aqueous solution of 1.5% w/w CMC, it shifts to a gas velocity slightly over this value.

To compare with transition conditions judged from a more classical procedure, the gas holdup is represented vs the gas velocity in Fig. 8, for experiments with water and with the CMC solution of highest viscosity. In this case, the gas holdup was determined by visual inspection of the disengagement region and by a scanning method using an external source to get a more objective reliable value, since the disengagement limit fluctuates strongly for high gas velocities. The figure provides results of a mean gas holdup across a section at the column mid-height. For all the model liquids used, three regions are apparent as previously found by other authors [5,13]. The first region, generally associated to the homogeneous regime is characterized by a linear relationship of the gas holdup with the gas velocity; then, a transition region is found for a range of gas velocities and finally, a less steeped region is observed in the gas holdup vs gas velocity curve for high gas velocities. The transition region may present discontinuities and increasing–decreasing trends depending mainly on liquid properties (viscosity, surface tension), on column size and on gas distributor. In this case, three linear trends are found, as observed for instance by Yang et al. [13]. For water, the homogeneous regime extends until gas velocities around 0.05 m/s, while the end of the transition seems to appear at gas velocities of 0.09 m/s. For the viscous non-Newtonian solution, the homogeneous regime apparently ends at lower gas velocities, around 0.035 m/s for the aqueous CMC solution of 0.75% w/w (not shown) and below 0.03 m/s for the 1.5% w/w CMC solution, pointing to a less stable homogeneous regime as the liquid viscosity increases. However, the end of transition, judged from the start of the linear trend at high gas velocities, is apparently reached for higher gas velocities as the liquid viscosity increases, at 0.095 m/s for the 0.75% w/w CMC solution and above 0.1 m/s for the most viscous liquid. Comparing with results shown in Fig. 7, the trend with gas velocity of symbol 192-frequency apparently indicates an intermediate

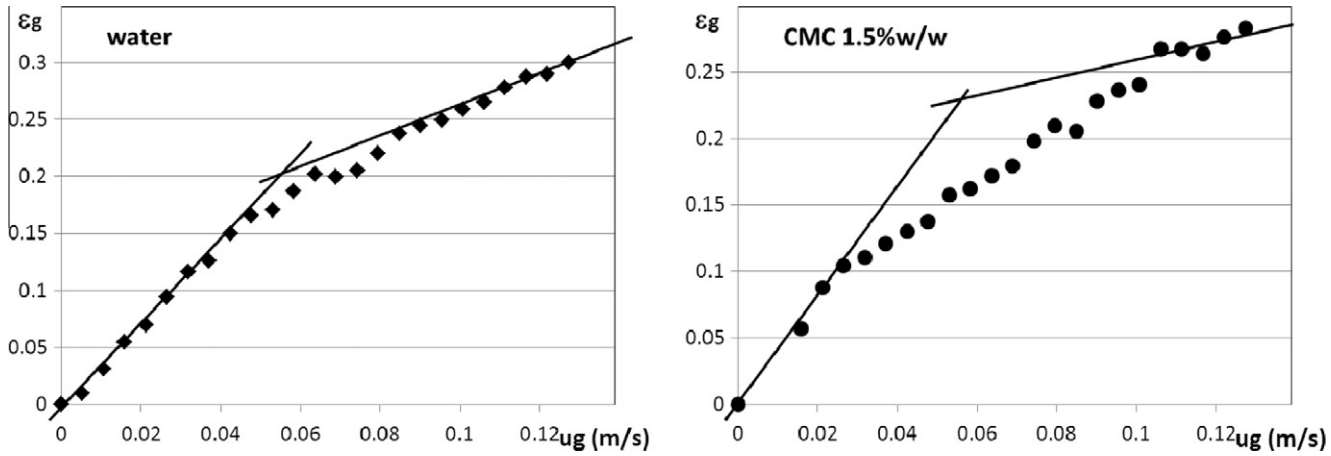

Fig. 8. Influence of gas velocity on the mean section gas holdup measured at column mid-height. Solid lines are only to guide the eyes for remarking the linear trends.

condition within the transition region. In the case of water, the value is close to the end of the homogeneous region, while for the viscous solutions it indicates a mean velocity within the transition region. In both cases, the break observed in Fig. 7 is close to the gas velocity arising from the intersection of the two extreme linear trends in the gas holdup vs gas velocity curve.

3.2.2. Dynamic symbolization

The symbols can also be defined based on a dynamic ground, pursuing exploration of persistent motions in a given direction compared to a fluctuating motion. The dynamic symbolization is generally appropriate to emphasize certain temporal patterns, like persistent trends, which are apparent in the analyzed time series, because the specific pattern is directly searched for. It has been suggested to be the preferred strategy when changes in time are more important than absolute measurements [7]. One way of dynamic symbolization is to directly assign a symbol to a particular trend of successive measurements. In this case, to define the symbols, five situations have been considered, taking into account three discrete axial positions of the tracer, separated by a time lag τ, according to the following rule:

- $z_i + \tau < z_i < z_i - \tau \Rightarrow$ a decreasing trend, symbol "-2" (1a)
- $z_i \leqslant z_i - \tau < z_i + \tau$ and $z_i < z_i + \tau \leqslant z_i - \tau \Rightarrow$ a trough, symbol "-1" (1b)
- $z_i - \tau = z_i = z_i + \tau \Rightarrow$ a stay, symbol "0" (1c)
- $z_i - \tau < z_i + \tau \leqslant z_i$ and $z_i + \tau < z_i - \tau \leqslant z_i \Rightarrow$ a peak, symbol "1" (1d)
- $z_i - \tau < z_i < z_i + \tau \Rightarrow$ an increasing trend, symbol "2" (1e)

After the time series of tracer axial coordinates is converted into a time series of symbols, the frequency of finding the corresponding symbol is computed. The histograms calculated from the experiments considering a time lag between observations of $\tau = 0.01$ s are illustrated in Fig. 9, for water and the most viscous CMC solution used, at four representative gas velocities.

From the figure, it is evident that when the lag among observations is very small, the most frequent recurrence corresponds to a stay; i.e., the three observations are in the same region. Note that the total observation window is only 0.03 s. This is also related to the resolution of the method, which depends on the number of detectors used. In this case, the number of detectors used define regions of 0.1 m in the axial coordinate. Symbols indicating a stay, a trough or a peak are not strongly dependent on the gas velocity and consequently on the underlying flow regime, since they are more related to instrumental noise and hydrodynamic local fluctuations and to the resolution of the method. On the contrary, symbols -2 and 2, which respectively point to a persistent decreasing and increasing trend, are markedly influenced by the gas velocity. This is especially evident in the case of the descending trends in the viscous non-Newtonian solutions, probably related to the more linear upward motion of the bubbles in non-Newtonian fluids, and wake characteristics that expel the liquid in the opposite direction, the so-called "negative wake" [4,14–16].

The frequency of symbol -2 (persistent descending path) and its trend with gas velocity is shown in Fig. 10 for water and for the aqueous solution of 1.5% w/w CMC. As mentioned before, there is a marked positive influence of the gas velocity on the frequency of

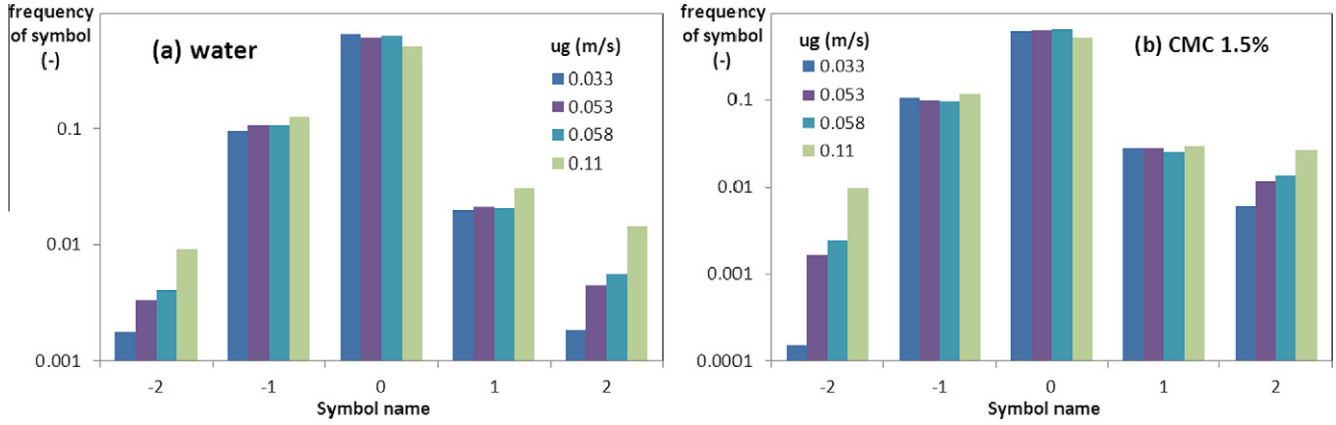

Fig. 9. Frequency of finding the symbols defined according to the dynamic symbolization rule (Eqs. (1a)–(1e)) for water and for the most viscous liquid examined, and four representative gas velocities.

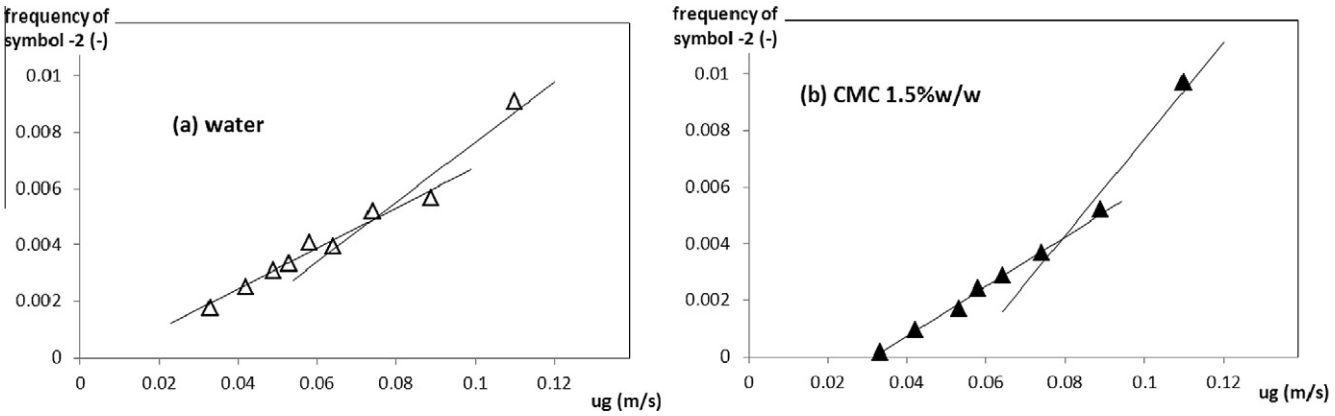

Fig. 10. Trend of the frequency of appearance of symbol −2 (a persistent descending motion) defined according to the dynamic symbolization rule. Solid lines are only to guide the eyes for remarking the break in the trend.

persistent descending paths. A break in the trend is evident for all the examined liquids and it has been remarked in the figure with solid lines arising from linear trends of the aligned values. In this case, the break is apparent for higher gas velocities than the ones pointed up by the static symbolization, remaining still within the transitions region diagnosed from the gas holdup vs gas velocity curve. From these quantifiers, the transition identified for the viscous liquid are slightly shifted to higher gas velocities compared to water.

Even if a break in the trend can be appreciated, the frequency of the symbol associated with persistent descending path is always very low, less than 1% of all the examined experimental conditions, since the observation window is too short. Increasing the considered time lag τ, an observation window more related to the time scale of the liquid motion can be examined. Therefore, Fig. 11 shows the trends with gas velocity of the frequency of the symbol associated with persistent descending paths for different time lags between 0.1 s to 1 s.

It can be observed that, for time lags between 0.3 s and 0.6 s (total observation windows of 0.6–1.2 s), there is always a break in the trend of symbol −2 frequency at a gas velocity around 0.05 m/s and the frequencies are between 2% and 10% of the total number of symbols, i.e., based on a more reliable statistics. These observation windows are appropriate to capture recurrent trends of persistent descending paths traversing maximum the whole column, since the frequency of the associated symbol is related to the liquid descending velocity. Larger observation windows are too long to catch the time scale of the liquid motion and the correlation is lost.

Based on results shown in Fig. 11 and considering that the liquid descending velocities are comparable for the viscous aqueous solutions of CMC, time lags of 0.3–0.4 s (observation windows of 0.6–0.8 s) have been considered to evaluate the transition for the viscous liquid solutions. The trends of the symbol associated with persistent descending paths for the aqueous solutions of CMC are shown in Fig. 12. For both liquid viscous solutions, the break in the trend appears for gas velocities above 0.06 m/s, within the transition region as inferred from the gas holdup vs gas velocity curve.

There is still no agreement on the effect of the non-Newtonian characteristics of the liquid on the flow transition between homogeneous and heterogeneous conditions in a bubble column since the experimental information available is limited, and due to the complex features of the phenomenon. It has been found that an increase in liquid viscosity can destabilized the homogeneous regime leading to flow transitions at lower gas velocities for moderately viscous Newtonian fluids, while for viscosities below a critical value, the homogeneous regime is stabilized [4,13,17]. For non-Newtonian fluids, the transition velocity has been found to increase with liquid elasticity [4] while it has also been argued that there could be no transition at all between homogeneous and heterogeneous flow regimes for very viscous non-Newtonian solutions [18]. For moderately viscous non-Newtonian fluids, the experimental variation of gas holdup with gas velocity reported by Fransolet et al. [18] could suggest that the transition conditions are not largely affected by the viscous character of the liquid, although the gas holdup decreases. On the contrary, Yang et al. [13] found a decrease on both of the transitions velocities (from homogeneous to transition and from transition to heterogeneous) as the liquid viscosity increases. Moreover, some authors [3,17] reported a complex dependence of the transition with the liquid viscosity, showing a maximum in the transition velocity vs liquid viscosity curve, and an effect of the relaxation time. From the experimental results presented in this work, the gas velocity indicating the end of the homogeneous regime decreases as the liquid viscosity increases, but the start of the completely heterogeneous regime is shifted to higher gas velocities for the higher viscosity non-Newtonian liquids. To completely establish the influence of liquid viscosity, particularly for non-Newtonian liquids, more research is still required.

From the symbolic analysis carried out, significant breaks have been found in the trends with gas velocity of different objective indexes that can be evaluated, related to the liquid level (thus, indirectly to the gas holdup) and to the liquid velocity. The found trends do not distinguish the transition region, they mostly indicate a unique transition velocity for conditions within the transition region judged from the gas holdup vs gas velocity curve. For the non-Newtonian aqueous CMC solutions, the transition between regimes estimated from the trend variations appears at slightly higher gas velocities than in water.

3.3. Residence time distributions

Considering time series of the tracer approximate axial location, as the one shown in Fig. 4, residence time distributions (RTDs) of the tracer at different axial regions can be determined. These RTDs have been obtained evaluating the time spent by the tracer at each region whenever it enters from any direction. Representative RTDs of the tracer, which in this case represents the liquid, for water and for an aqueous solution of CMC (1.5% w/w) are shown, respectively, in Figs. 13 and 14 for four regions along the column and three gas velocities. Regions in the column, indicated with detectors number, expand 0.1 m for detectors 2–7 and 0.15 m for detector 1. Hence, region expressed by Detector 1 corresponds to axial locations below 0.15 m; by Detector 2, axial positions between 0.15 and 0.25 m; Detector 3, axial positions between 0.25 and 0.35 m, etc. Detector 8 is not considered since the gas–liquid emulsion level does not completely cover it.

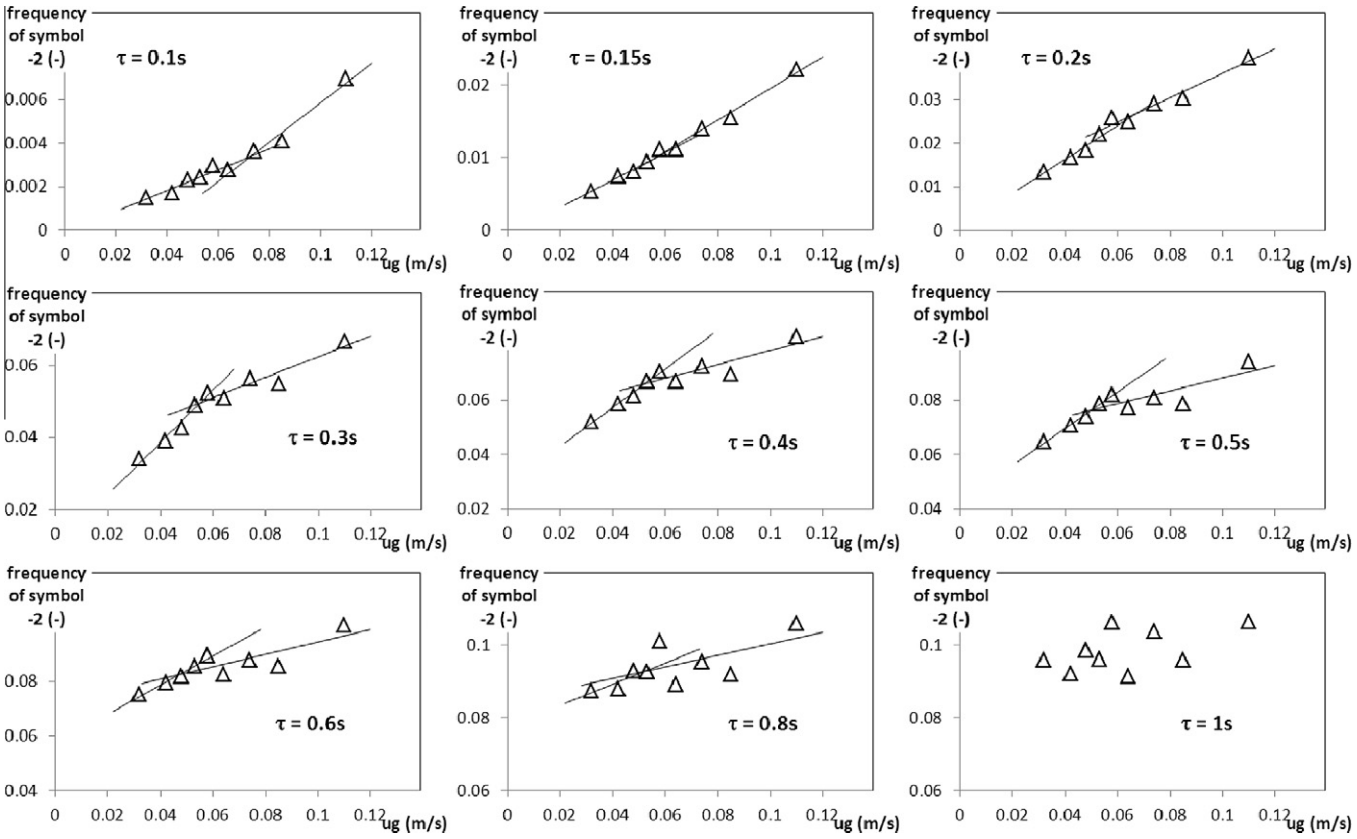

Fig. 11. Trend of the frequency of appearance of symbol −2 (a persistent descending motion) defined according to Eqs. (1a)–(1e) for different time lags τ between observations. Liquid: water. Solid lines are only to guide the eyes for remarking the break in the trend and they are calculated as linear trends of the aligned points.

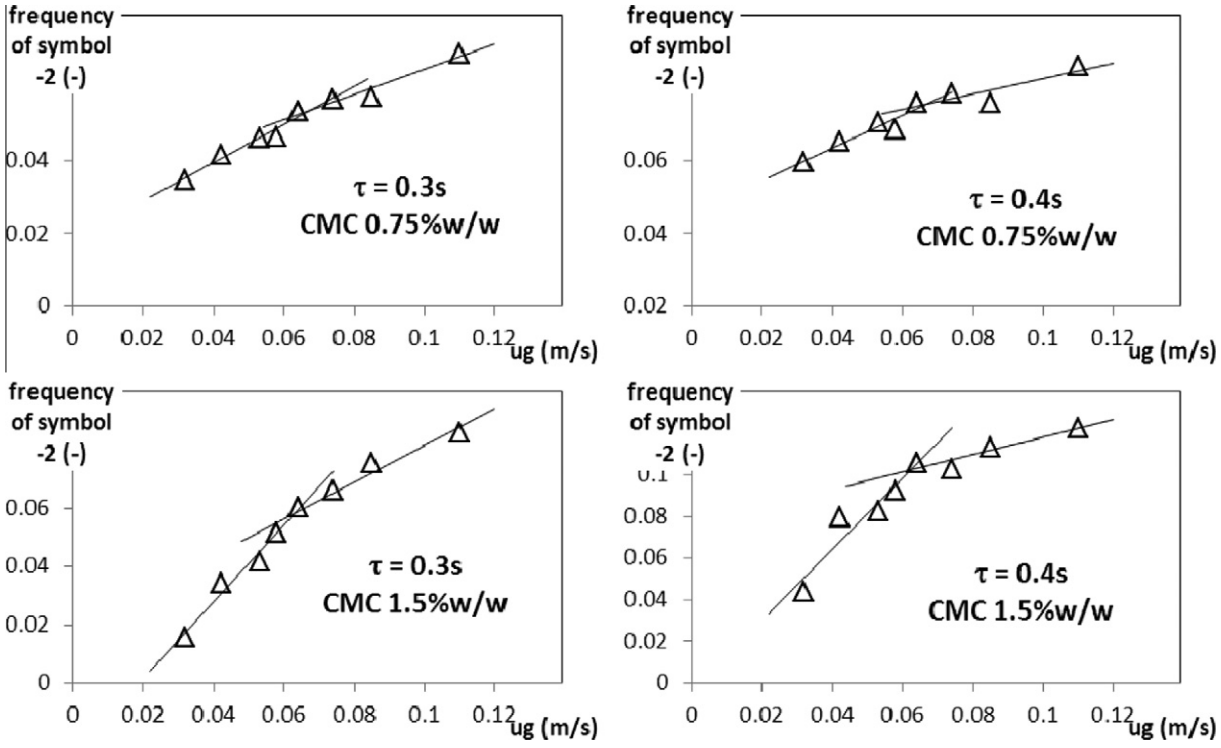

Fig. 12. Trend of the frequency of appearance of symbol −2 (a persistent descending motion) defined according to Eqs. (1a)–(1e) for different time lags τ between observations. Liquid: aqueous solutions of CMC. Solid lines are only to guide the eyes for remarking the break in the trend and they are calculated as linear trends of the aligned points.

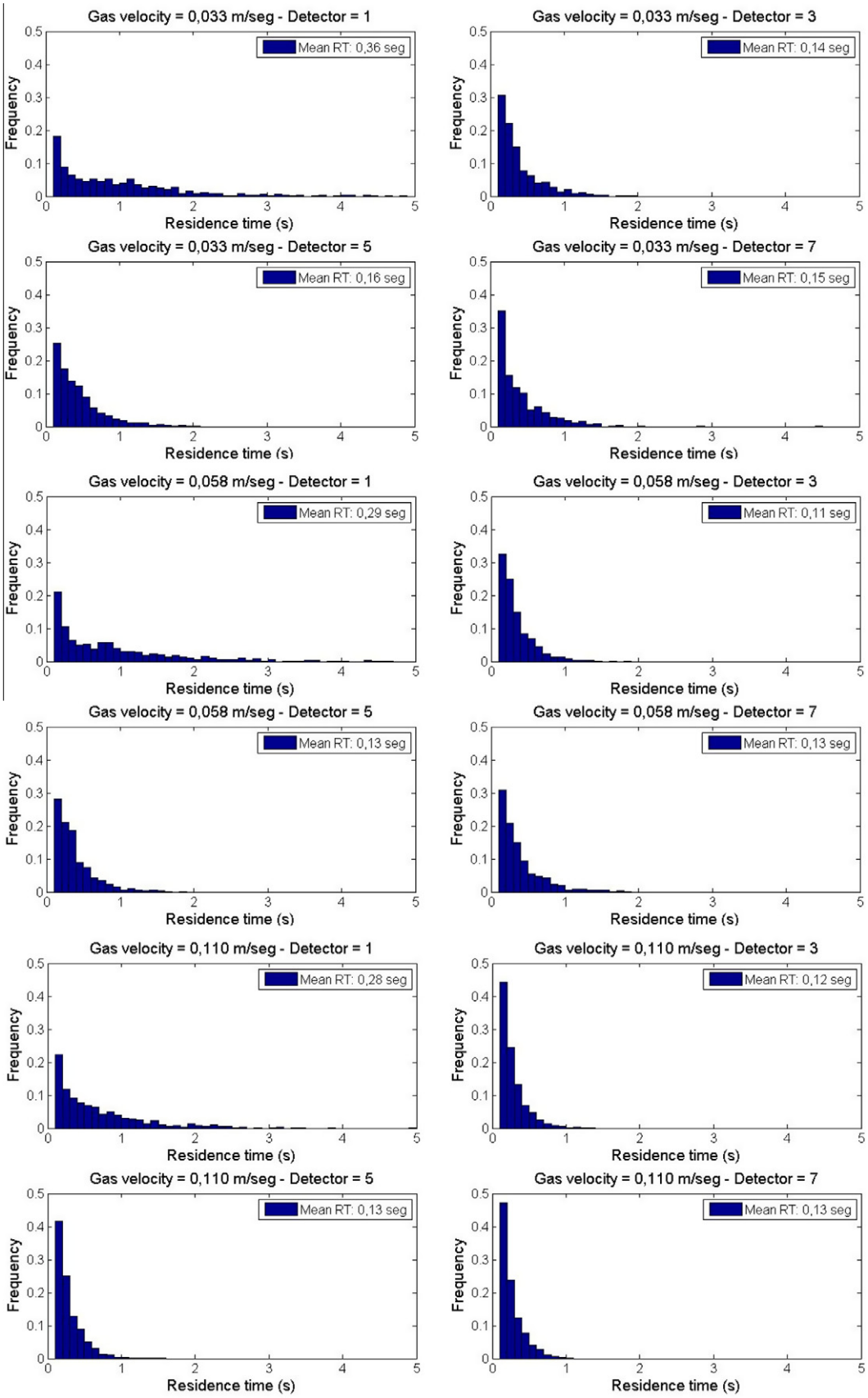

Fig. 13. Residence time distributions of the tracer at four regions within the column for three gas velocities. Liquid: water. The number of detector indicates the region of the column observed; all the regions have 0.1 m length except the one for detector 1, which has 015 m. See Fig. 1 for a schematic of detector location.

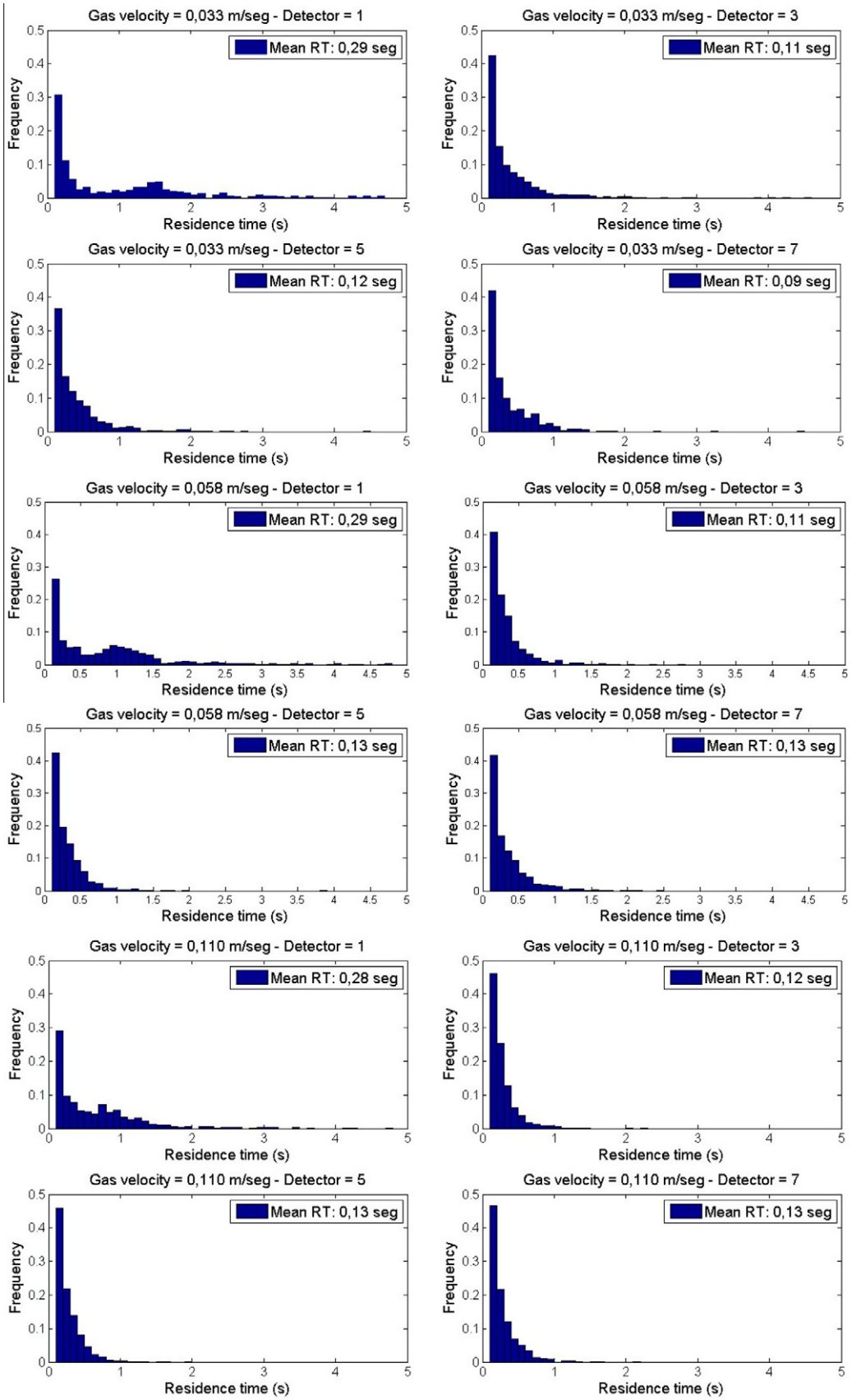

Fig. 14. Residence time distributions of the tracer at four regions within the column for three gas velocities. Liquid: aqueous solution of CMC 1.5% w/w. The number of detector indicates the region of the column observed; all the regions have 0.1 m length except the one for detector 1, which has 015 m. See Fig. 1 for a schematic of detector location.

As observed from the figures, the residence time distributions are not strongly influenced by gas velocity, being slightly narrower only for the higher gas velocity examined. For the more viscous solution, the frequency of very short residence times decreases with respect to water but the mean residence times are similar, except for the lower gas velocity. For this condition, the mean residence times are lower in water than in the viscous solution.

The tracer remains relatively longer periods in the bottom of the column than in the other regions, leading to broader residence time distributions, probably captured in the vortex that arise from the gas jets in the entrance region. As a consequence, the mean residence time of the tracer in the entrance region is almost two times the value determined in other regions of 0.1 m along the column, which is generally around 0.13 s.

4. Conclusions

The feasibility of inferring information of the underlying dynamics in bubble columns, using a set of axially aligned detectors (AADs) that scan simultaneously different column heights when a unique radioactive tracer is left free within the examined vessel is demonstrated. The combined response of the AADs allows reconstructing the approximate axial trajectory of the tracer along the column.

The time series of intensities registered by the AADs can be analyzed by means of a data symbolization procedure to determine quantitative indexes related to the underlying flow regime. Quantitative indexes defined by static and dynamic symbolization rules present a break in their trends with gas velocity suggesting their ability to diagnose a flow transition. This flow transition is found at slightly higher gas velocities in the case of viscous non-Newtonian fluids compared to water.

Residence time of the tracer in the entrance region of the column is significantly higher than in the rest of the column. The mean residence times at different column regions are not strongly affected by the gas velocity or by the liquid characteristics.

Acknowledgements

Financial support from CONICET and Universidad de Buenos Aires are gratefully acknowledged. G.Salierno, M.Cassanello, M.A.Cardona and D. Hojman are members of CONICET. We would particularly like to thank the staff of the RA1 reactor of CNEA, Argentina, for the activation of the sources used in this work.

References

[1] N. Kantarci, F. Borak, K.O. Ulgen, Review: bubble column reactors, Process Biochem. 40 (2005) 2263–2283.
[2] M.P. Dudukovic, Opaque multiphase flows: experiments and modelling, Exp. Thermal Fluid Sci. 26 (2002) 747–761.
[3] J. Chaouki, F. Larachi, M.P. Dudukovic, Non-Invasive Monitoring of Multiphase Flow, Elsevier, Amsterdam, The Netherlands, 1997.
[4] G. Olivieri, M.E. Russo, M. Simeone, A. Marzocchella, P. Salatino, Effects of viscosity and relaxation time on the hydrodynamics of gas–liquid systems, Chem. Eng. Sci. 66 (2011) 3392–3399.
[5] A. Shaikh, M.H. Al Dahhan, A review on flow regime transition in bubble columns, Int. J. Chem. React. Eng. 5 (2007) R1.
[6] M.S. Fraguío, M.C. Cassanello, F. Larachi, J. Chaouki, Flow regime transition pointers in three-phase fluidized beds inferred from a solid tracer trajectory, Chem. Eng. Process. 45 (2006) 350–358.
[7] C.S. Daw, C.E.A. Finney, E.R. Tracy, A review of symbolic analysis of experimental data, Rev. Sci. Instrum. 74 (2003) 915–930.
[8] F. Larachi, G. Kennedy, J. Chaouki, A g-ray detection system for 3-D particle tracking in multiphase reactors, Nucl. Instrum. Methods Phys. Res., Sect. A 338 (1994) 568–576.
[9] S. Bhusarapu, M.C. Cassanello, M. Al-Dahhan, M.P. Dudukovic, S. Trujillo, T. O'Hern, Dynamical features of the solid motion in gas-solid risers, Int. J. Multiphase Flow 33 (2007) 164–181.
[10] V. Rajagopalan, A. Ray, R.R. Samsi, J. Mayer, Patter identification in dynamical systems via symbolic time series analysis, Pattern Recogn. 40 (2007) 2897–2907.
[11] S. Gupta, A. Ray, E. Keller, Symbolic time series analysis of ultrasonic signals for fatigue damage monitoring in polycrystalline alloys, Meas. Sci. Technol. 17 (2006) 1963–1973.
[12] J.G. Brida, L.F. Punzo, Symbolic time series analysis and dynamic regimes, Struct. Change Econ. Dyn. 14 (2003) 159–183.
[13] J.H. Yang, J.-I. Yang, H.-J. Kim, D.H. Chun, H.-T. Lee, H. Jung, Two regime transitions to pseudo-homogeneous and heterogeneous bubble flow for various liquid viscosities, Chem. Eng. Process. 49 (2010) 1044–1050.
[14] D. Funfschilling, H.Z. Li, Flow of non-Newtonian fluids around bubbles: PIV measurements and birefringence visualization, Chem. Eng. Sci. 56 (2001) 1137–1141.
[15] M. Kemiha, X. Frank, S. Poncin, H.Z. Li, Origin of the negative wake behind a bubble rising in non-Newtonian fluids, Chem. Eng. Sci. 61 (2006) 4041–4047.
[16] J.R. Herrera-Velarde, R. Zenit, D. Chehata, B. Mena, The flow of non-Newtonian fluids around bubbles and its connection to the jump discontinuity, J. Non-Newtonian Fluid Mech. 111 (2003) 199–209.
[17] M.C. Ruzicka, J. Drahoš, P.C. Mena, J.A. Teixeira, Effect of viscosity on homogeneous–heterogeneous flow regime transition in bubble columns, Chem. Eng. J. 96 (2003) 15–22.
[18] E. Fransolet, M. Crine, P. Marchot, D. Toye, Analysis of gas holdup in bubble columns with non-Newtonian fluid using electrical resistance tomography and dynamic gas disengagement technique, Chem. Eng. Sci. 60 (2005) 6118–6123.